CEP63 deficiency promotes p53-dependent microcephaly and reveals a role for the centrosome in meiotic recombination

Marko Marjanovi [1,2], **Carlos Sánchez-Huertas**[1,#], **Berta Terré**[1,#], **Rocío Gómez**[3], **Jan Frederik Scheel**[4,5], **Sarai Pacheco**[6,7], **Philip A. Knobel**[1], **Ana Martínez-Marchal**[6,7], **Suvi Aivio**[1], **Lluís Palenzuela**[1], **Uwe Wolfrum**[4], **Peter J. McKinnon**[8], **José A. Suja**[3], **Ignasi Roig**[6,7], **Vincenzo Costanzo**[9,*], **Jens Lüders**[1,*], and **Travis H. Stracker**[1,*]

[1]Institute for Research in Biomedicine (IRB Barcelona), 08028 Barcelona, Spain

[2]Division of Molecular Medicine, Ru er Boškovi Institute, 10000 Zagreb, Croatia

[3]Departamento de Biología, Edificio de Biológicas, Universidad Autónoma de Madrid, 28049 Madrid, Spain

[4]Department of Cell and Matrix Biology, Institute of Zoology, Johannes Gutenberg University, 55122 Mainz, Germany

[6]Genome Integrity and Instability Group, Institut de Biotecnologia i Biomedicina, Universitat Autònoma de Barcelona, 08193 Cerdanyola del Vallès, Spain

[7]Cytology and Histology Unit, Department of Cell Biology, Physiology and Immunology, Universitat Autònoma de Barcelona, 08193 Cerdanyola del Vallès, Spain

[8]Department of Genetics, St. Jude Children's Research Hospital, 38105 Memphis, TN, USA

[9]FIRC Institute of Molecular Oncology, 20139 Milan, Italy

Abstract

CEP63 is a centrosomal protein that facilitates centriole duplication and is regulated by the DNA damage response. Mutations in *CEP63* cause Seckel syndrome, a human disease characterized by microcephaly and dwarfism. Here we demonstrate that *Cep63* deficient mice recapitulate Seckel syndrome pathology. The attrition of neural progenitor cells involves p53-dependent cell death and brain size is rescued by the deletion of p53. Cell death is not the result of an aberrant DNA

*To whom correspondence should be addressed: Travis Stracker, Travis.Stracker@irbbarcelona.org, Jens Lüders, Jens.Luders@irbbarcelona.org, Vincenzo Costanzo, Vincenzo.Costanzo@ifom.eu.
[5]Present address: Department of Multiphase Chemistry, Max Planck Institute for Chemistry, 55128 Mainz, Germany
#These authors contributed equally to the manuscript.

Author Manuscript Author Manuscript Author Manuscript Author Manuscript

damage response but is triggered by centrosome-based mitotic errors. In addition, *Cep63* loss severely impairs meiotic recombination, leading to profound male infertility. *Cep63* deficient spermatocytes display numerical and structural centrosome aberrations, chromosome entanglements and defective telomere clustering, suggesting that a reduction in centrosome-mediated chromosome movements underlies recombination failure. Our results provide novel insight into the molecular pathology of microcephaly and establish a role for the centrosome in meiotic recombination.

Keywords

centrosome; centriole; microcephaly; fertility; meiosis

Introduction

Many mutations in genes encoding proteins involved in the DNA damage response (DDR) and/or centrosomal functions have been identified in human patients with autosomal recessive primary microcephaly (MCPH) or Seckel syndrome (MCPH accompanied by dwarfism)[1–13]. This has suggested that crosstalk between the DDR and the centrosome may be highly relevant to the etiology of microcephaly. Supporting this idea, several MCPH/Seckel proteins, such as MCPH1 and CEP152, have been implicated in both centrosomal and DDR functions[9, 14–16]. In addition, signaling through the central transducer of DNA damage, ATR (also mutated in Seckel syndrome), involves the PCNT/MCPH1 dependent localization of CHK1 to the centrosome[17, 18].

The development of microcephaly has been attributed to the attrition of neural progenitor cells (NPCs) due to defective self-renewal capacity or as a result of sporadic DNA damage, resulting from checkpoint defects, DNA repair deficiencies, replication stress, mitotic errors and increased apoptosis[4, 19]. In addition, defective nuclear partitioning and the death of migrating differentiated cells have also been shown to influence cortical development[20]. The relative importance of these, or other mechanisms, in the pathology of microcephaly in MCPH and Seckel syndrome, and to what extent other organ systems are affected, remain open questions.

The centrosomal protein CEP63 was identified as a target of the apical DDR kinases ATM and ATR in mitosis and was recently shown to promote efficient centriole duplication through interactions with CEP152, which has also been implicated in ATM signaling[5, 9, 21, 22]. Both *CEP63* and *CEP152* mutations have been identified in Seckel syndrome and additional *CEP152* mutations underlie MCPH[5, 7, 9].

Here we describe the phenotypic analysis of mice lacking expression of the *Cep63* gene. These animals recapitulate the pathological outcomes reported in human patients with *CEP63* mutations, including growth defects and microcephaly[5]. Brain development in *Cep63* mutants is impaired by increased cell death and reduced numbers of NPCs, which can be rescued by the deletion of *p53*, but not the ATM or CHK2 kinases. *Cep63* deficient cells and tissues do not show obvious defects in DNA damage signaling, but exhibit impaired centriole duplication accompanied by defects in bipolar spindle assembly and function.

Additionally, we find that male *Cep63* deficient mice are infertile, exhibiting severe defects in meiotic recombination and a complete block in the generation of mature sperm. We show that in spermatocytes, centrosome duplication is coordinated with the progression of meiotic prophase. In *Cep63* deficient males, centrosomes fail to duplicate and display compromised structural integrity, and chromosome dynamics are impaired. Collectively our results shed light on the complex etiology of microcephaly and reveal a novel and essential role for centrosomes in promoting recombination during mammalian meiosis.

Results

Cep63 deficiency leads to growth defects and microcephaly

Previous work demonstrated an interaction between CEP63 and CEP152, two proteins encoded by established MCPH and Seckel Syndrome genes[5, 9, 22, 23]. To determine if *Cep63* deficiency in mice would phenocopy the human diseases, we generated animals with a gene-trapped allele of the *Cep63* gene (*Cep63^T*)[22]. *Cep63$^{T/T}$* pups were born at expected Mendelian ratios and newborn animals were similar in weight to wild type (*WT*) or heterozygous littermates (Fig. 1a). However, by 1 to 2 months, *Cep63$^{T/T}$* mice exhibited a significant reduction in the average weight (Fig. 1b and 1c), indicating growth retardation, a hallmark of human Seckel syndrome patients[3, 5, 9].

As *CEP63* mutations cause microcephaly in humans[5], we examined neurodevelopment in *Cep63$^{T/T}$* animals. In newborn (p2) animals, forebrain size was reduced compared to *WT*, despite similar body weight (Fig. 1d and 1a). Strongly reduced *Cep63* mRNA levels were confirmed in the cortex of *Cep63$^{T/T}$* mice (Fig. 1e) while *Anapc13*, a gene positioned head-to-head with *Cep63*, was not affected. In addition we did not observe changes in the expression of key centriole duplication components *Plk4* and *Cep152*, or the *Cep63* paralogue, *Deup1* (Fig. 1e). Characteristic of MCPH and Seckel syndrome, cortical development was impaired (Fig. 1f) and examination of p2 cortices revealed a consistent reduction in thickness at all positions examined (Fig. 1g). Despite reduced cortex size, longevity of *Cep63$^{T/T}$* animals was similar to *WT* and no obvious motor defects were observed in an aging cohort (Fig. 1h). Together, these data demonstrated that *Cep63* deficiency recapitulated the major pathologies of Seckel Syndrome.

Mitotic defects and cell death in neural progenitors

The attrition of NPCs in the cortex has been clearly linked to microcephaly, and can be provoked by increased DNA damage, impaired NPC self-renewal or centrosomal defects[24–27]. CEP63 has been linked to the DNA damage response and its deficiency leads to centriole loss due to impaired recruitment of CEP152[5, 22]. We therefore examined colocalization of CEP152 or CEP63 with the centrosome marker γ-tubulin in the developing cortex of E14.5 embryos[5, 22]. While focal CEP152 was readily detected at centrosomes in *WT* animals, we could not identify focal staining that overlapped with γ-tubulin in *Cep63$^{T/T}$* mice (Fig. 2a). Since *Cep152* mRNA expression levels in the *Cep63$^{T/T}$* brain were not reduced relative to *WT* (Fig. 1e) and similar amounts of CEP152 protein could be immunoprecipitated from *WT* and *Cep63$^{T/T}$* tissues (Supplementary Fig. 1), this likely reflects a defect in the centrosomal recruitment of CEP152, similar to what we have

previously reported in *Cep63*$^{T/T}$ MEFs[22]. In addition, while we could readily detect CEP63 localization to the centrosomes in *WT* E14.5 embryos, we did not observe its localization in *Cep63*$^{T/T}$ embryos, consistent with its reduced levels of expression (Fig. 1e, Fig. 2b and Supplementary Fig. 1).

As defective CEP63/CEP152 recruitment and impaired centriole duplication could lead to mitotic defects, we next examined the status of the proliferative NPC population and cell death in the developing cortex of E14.5 animals using antibodies against histone H3 phosphorylated on Serine10 (p-H3Ser10), a marker of mitosis, and the apoptotic marker cleaved caspase-3. At E14.5 we observed slightly elevated numbers of p-H3Ser10 positive cells in the ventricular zone (VZ) of the cortex of *Cep63*$^{T/T}$ animals compared to *WT* (Fig. 2c and 2d) and highly elevated levels of cleaved caspase 3 throughout the cortex (Fig. 2e). In addition, we observed an increased number of extra-VZ p-H3Ser10 positive cells, similar to what has been recently reported in mice lacking SAS4 (Fig. 2c and 2d)[25]. We examined the identities of these misplaced proliferating cells using a marker for intermediate progenitors (IPs), Tbr2, and found that this displaced population was composed of both Tbr2 positive and negative cells suggesting that it is composed of multiple classes of NPCs, including radial glial progenitors (RGPs) and IPs (Fig. 2f).

The increased number of mitotic cells, coupled with the increased cell death we observed, suggested the presence of mitotic errors or delays. We next examined the spindle configurations in *WT* and *Cep63*$^{T/T}$ cortices using anti-γ-tubulin antibodies and DAPI, to label centrosomes and DNA respectively. This revealed a strong increase in the percentage of monopolar spindle configurations in the ventricular zone (VZ) of *Cep63*$^{T/T}$ cortices (Fig. 2g). Moreover, in cells with bipolar spindles, the γ-tubulin signal at one of the poles was frequently dim or absent, suggesting that spindle poles were formed by defective centrosomes or were acentrosomal (Fig. 2h and 2i). Collectively, these data indicated that CEP63 ensures proper duplication and formation of functional centrosomes, which in NPCs is crucial for mitotic fidelity, proper positioning of proliferating NPCs and cell survival.

Cep63 deficiency leads to p53-dependent NPC attrition

NPCs lacking centrioles are misplaced from the subventricular zone (SVZ), exhibit prolonged mitoses, and trigger cell death through p53 signaling[26, 28, 29]. However, opposing genetic interactions with *p53* deficiency have been described in other models of microcephaly, such as in *Atr* deficient mice, and CEP63 has been previously linked to the ATM/ATR-dependent DNA damage response[24, 28, 30, 31]. To address the cell death pathways triggered by loss of CEP63, we stained the cortices of E14.5 mice with antibodies for the DNA break marker γH2AX or p53. Little staining for either marker was observed in *WT* animals while a striking upregulation of p53 was apparent in the cortex of *Cep63*$^{T/T}$ embryos (Fig. 3a to 3d). The majority of p53 staining was observed in the PCNA positive cells of the VZ, suggesting that p53 is primarily activated in the proliferating NPC population (Fig. 3b). Only a minor increase in γH2AX was seen in the cortex of *Cep63*$^{T/T}$ animals but the staining was not punctate, as expected for DNA breaks, and may reflect cells already undergoing apoptosis (Fig. 3c and 3d).

To determine if p53 activation was sufficient to drive NPC attrition in *Cep63*[T/T] mice, we intercrossed them with *p53*^{−/−} animals. Strikingly, we observed a complete rescue of brain size in *Cep63*[T/T] *p53*^{−/−} mutants (Fig. 3e, 3f and 3g). Consistent with these observations, TUNEL staining revealed increased numbers of apoptotic cells in E14.5 cortices of *Cep63*[T/T] mice, which was rescued by loss of p53 (Fig 3h). To determine if the loss of p53 rescued the proliferating NPC population, we stained the cortex with antibodies for the NPC marker SOX2 and quantified cell number (Fig. 3i and 3j)[32]. In the *Cep63*[T/T] cortex we found a reduced total number of SOX2+ cells but an increased percentage that were mislocalized (Fig. 3j). The reduction of NPC number in *Cep63*[T/T] mice was rescued by p53 but the majority of the rescued NPCs were misplaced from the VZ (extra-VZ), consistent with the loss of this misplaced progenitor population underlying the microcephaly phenotype (Fig. 3i and 3j).

In response to DNA double-strand breaks, the CHK2 and ATM kinases play important roles in mediating p53 dependent apoptosis[33]. However, in contrast to p53 deficiency, neither the loss of CHK2 or ATM rescued the reduced brain size observed in *Cep63*[T/T] animals (Fig. 3f and 3g). This suggested that chromosome breaks are unlikely to be a primary trigger for p53 activation and cellular attrition *in vivo*, consistent with the lack of extensive γH2AX staining (Fig. 3c and 3d). In addition, we have observed normal ATM/ATR-dependent DNA damage responses (DDR) in MEFs and intact physiological repair in the immune system of *Cep63*[T/T] mice (Supplementary Fig. 2). Collectively our data showed that CEP63 deficiency causes centrosomal defects that lead to mitotic errors and misplacement of NPCs, triggering p53-mediated cell death and microcephaly.

Severe defects in testes development and male infertility

While our assays failed to detect clear DDR defects in the brain (Fig. 3c and 3d) or other tissues (Supplementary Fig. 2), we next examined fertility, as germ line meiotic recombination is mediated by proteins largely distinct from those required for NHEJ and immune system development, and is often affected in genetic instability disorders[33]. We found that *Cep63*[T/T] females were fertile and generated litter sizes comparable to those of *WT* animals (Supplementary Fig. 3). However, histological examination found a reduction in oocytes, even though follicles at all stages were present (Supplementary Table 1). In contrast, despite copulation, no *WT* females were impregnated by *Cep63*[T/T] males. We observed a progressive reduction in testis size in *Cep63*[T/T] males, which was apparent in 10-day old (p10) but more dramatic in 5.5 month old (p165) animals (Fig. 4a) and was independent of p53, ATM or CHK2 (Supplementary Fig. 4). Examination of 5-day old (p5) *Cep63*[T/T] animals revealed reduced cellularity but proportionally normal numbers of spermatagonia (Fig. 4b). In addition, we could occasionally identify polyploid spermatagonia in testes squash preparations, suggesting defective primordial germ cell expansion during development (Fig. 4b). Testes of p60 *Cep63*[T/T] animals contained numbers of tubules comparable to *WT* but tubule diameter and cellularity were reduced (Fig. 4c, 4d and Supplementary Fig. 4), most likely due to increased cell death (Fig. 4e and 4f). Few spermatids were visible in *Cep63*[T/T] testes sections and rare elongated spermatids were identified in testes squash preparations, but all appeared morphologically abnormal, in some cases exhibiting defective DNA compaction as sperm tails stained with DAPI (Fig. 4g).

Further, sperm counts from the dissected vas deferens showed that $Cep63^{T/T}$ mice had no identifiable sperm, indicating that the rare $Cep63^{T/T}$ spermatids did not leave the testes (Fig. 4h). These results suggested that CEP63 deficiency impairs spermatogenesis at multiple stages.

CEP63 is required for male meiotic recombination

As the position of TUNEL positive cells in seminiferous tubules (Fig. 4e) was consistent with that of the meiotic population, we examined meiotic progression using markers for the lateral and central elements of the synaptonemal complex (SCP3 and SCP1, respectively). Compared to *WT*, $Cep63^{T/T}$ mice showed increased leptotene and zygotene stage cells, similar numbers of pachytene cells, but very few cells (4%) that progressed to diplotene (Fig. 5a). This suggested that defects in the early stages of meiotic prophase I delayed progression to later stages and/or there was progressive cell loss during prophase I.

The efficient generation of DSBs in leptotene and their subsequent repair is required for timely homologue pairing, synapsis and meiotic prophase progression[34, 35]. We examined the number of DSBs generated during prophase I by counting the number of foci of the repair proteins RAD51 and DMC1. Increased numbers of RAD51 and DMC1 foci were observed from leptotene to zygotene in $Cep63^{T/T}$ mice compared to *WT* (Fig. 5b and 5c) suggesting that formation of DSBs was not defective, but their resolution potentially was. In $Cep63^{T/T}$ cells that progressed to pachytene, foci were largely resolved to similar levels as in *WT*. However, many pachytene and diplotene cells exhibited diffuse γH2AX staining that was not confined to the sex-body, consistent with delayed repair (Fig 5d). We also identified numerous abnormal or apoptotic cells with zygotene and pachytene like SC patterns (H1t negative, a marker of late pachytene) that were absent in controls (Fig. 5e). These included apparent SC entanglements and chromosome fusions, as well as ring γH2AX staining, indicative of programmed cell death (Fig. 5e).

We next examined crossover (CO) formation, one of the outcomes of meiotic recombination, using MLH1 as a marker. In contrast to *WT*, the majority of pachytene cells from male $Cep63^{T/T}$ mice lacked detectable MLH1 foci (Fig. 5f) indicating that they did not progress past early pachytene, an observation corroborated by H1t staining (Supplementary Fig. 4). In cases where MLH1 foci were present, higher numbers of COs per autosome (Fig. 5g) and longer SCs were detectable (Supplementary Fig. 4), reinforcing a role for CEP63 in the completion of male meiotic recombination. In contrast, comparable numbers of MLH1 foci were observed in *WT* and $Cep63^{T/T}$ females, supporting a sex specific role for CEP63 during meiotic prophase I progression (Fig. 5g). Thus, the loss of CEP63 led to male specific meiotic recombination defects, cell death and infertility.

Impaired centriole duplication in CEP63 deficient cells

As the severe recombination defect we observed was unexpected given that we have not detected sensitivity to DNA damage or nuclear localization of CEP63 or CEP152 in other tissues, we examined their localization throughout prophase I using SCP3 as a marker. Regardless of the stage, CEP63 or CEP152 localization was restricted to centrosomes, identified by staining with PCNT (Fig. 6a). Consistent with what we observed in all other

cell types and tissues we have examined, centrosomal CEP63 and CEP152 was not detected in prophase I spermatocytes in the testes of *Cep63$^{T/T}$* mice (Fig. 6a).

During meiotic prophase, membrane spanning Linker of Nucleoskeleton and Cytoskeleton (LINC) complexes containing SUN and KASH domain proteins tether chromosomes to the inner nuclear envelope and mediate interactions with the microtubule cytoskeleton at the cytoplasmic side[36]. This linkage drives chromosome movements and facilitates correct meiotic homologue pairing and recombination[37–40]. We therefore speculated that recombination failure in *Cep63$^{T/T}$* males could be due to aberrant centrosomes. To address this we first characterized centriole duplication in *WT* spermatocytes since, to our knowledge, the unperturbed centrosome configuration in mouse prophase I spermatocytes had not been reported previously. By staining with antibodies against pericentrin (PCNT) and centrin 3 to label centrosomes and centrioles, and SCP3 antibodies for meiotic staging, we found that early prophase I spermatocytes presented a single centrosome (single PCNT-positive foci) with unduplicated centrioles (two small centrin-positive dots adjacent to the larger PCNT foci) (Fig. 6b, 6c and Supplementary Fig. 5). At later stages, centriole numbers increased, and only by pachytene/diplotene, centriole duplication was completed (four centrin dots) (Fig. 6c and Supplementary Fig. 5). Separation of duplicated centrosomes occurred only at the end of prophase I or early in prometaphase I (Supplementary Fig. 5). Consistent with this, CEP63 and CEP152, which are associated with the proximal end of mother centrioles[5], localized as two foci that remained paired from leptotene through pachytene (Fig. 6a). Interestingly, staining with anti-NEDD1 or anti-γ-tubulin antibodies, which detect the microtubule nucleating γ-tubulin ring complex, was relatively dim and restricted to the centrioles throughout prophase I (Supplementary Fig. 5). Together the data suggests that contrary to the situation in most somatic cells, centrosome duplication and separation in mouse spermatocytes are delayed such that duplication is initiated in early prophase I and duplicated centrosomes are not separated before the end of prophase I.

To validate these findings we employed transmission electron microscopy (TEM). Consistent with the immunofluorescence results, *WT* spermatocytes in leptotene always contained a single centrosome with unduplicated centrioles (Fig. 6d). Only at zygotene/ pachytene could short daughter centrioles growing from the wall of mother centrioles be observed (Fig. 6d). By metaphase I, mothers and elongated daughters that appeared disengaged were present at spindle poles (Supplementary Fig. 5). This was consistent with previous work that reported essentially the same pattern of delayed centriole duplication and centrosome separation in hyrax and squirrel spermatocytes[41].

Next we analyzed centrosomes in *Cep63$^{T/T}$* spermatocytes. In contrast to *WT* cells, many *Cep63$^{T/T}$* cells had only one or no detectable centriole at leptotene, and most existing centrioles failed to duplicate during prophase I. As a result, by pachytene/diplotene *Cep63$^{T/T}$* cells contained on average only two centrioles whereas *WT* cells contained four (Fig. 6c and Supplementary Fig. 5). TEM analysis confirmed the presence of only one or two single centrioles in leptotene (Fig. 6d). Interestingly, in cells with two centrioles these appeared to be slightly further apart than in *WT* cells (Fig. 6d). Strikingly, we never observed growing or fully-grown daughter centrioles at later stages. Despite the duplication defect, the existing centrioles in *Cep63$^{T/T}$* cells appeared to be of normal size and structure,

consistent with previous results in chicken DT40 cells lacking CEP63 (Supplementary Fig. 6)[5].

Apart from impairing centriole duplication CEP63 deficiency also seemed to affect centrosome integrity. PCNT staining of *WT* centrosomes revealed an irregularly shaped but compact pericentriolar material (PCM), that in most cells had one or two extrusions (Fig. 6e, f, g). The identity and distribution of the PCM was confirmed by two independent markers, CDK5RAP2 and PCNT, which largely colocalized (Fig. 6e). Compared to *WT* cells, the PCM of centrosomes in *Cep63^{T/T}* spermatocytes appeared less compact, with a less intensely stained central region ("hollow") and an increase in extrusion number (Fig. 6b, e–h). However, total levels of PCNT at centrosomes were similar in *WT* and *Cep63^{T/T}* spermatocytes (Supplementary Fig. 6). Very similar PCM perturbations in *Cep63^{T/T} cells* were revealed by staining with CDK5RAP2 antibodies (Supplementary Fig. 6). Together, these data indicated that in spermatocytes, CEP63 was crucial for centriole duplication during meiotic prophase I and that, even though centriolar ultrastructure appeared normal, most centrosomes lacking CEP63 displayed abnormal PCM organization.

Telomere clustering defects in CEP63 deficient cells

As a direct role for CEP63/CEP152 in meiotic recombination seemed unlikely given the lack of detectable nuclear localization, we asked whether aberrant centrosomes in *Cep63^{T/T}* cells impair chromosome movements required for recombination. Such a defect could be caused by loss of chromosome attachment to the nuclear envelope or lack of tethering to the microtubule cytoskeleton by LINC complexes[40, 42, 43]. In *Cep63^{T/T}* spermatocytes, SUN1, the telomeric SUN domain protein that mediates attachment of chromosomes to the inner nuclear envelope, was localized to telomeres, and the distribution of TRF1 (telomeric marker) was consistent with nuclear envelope localization (Fig. 7a), suggesting that chromosome attachment was intact. We next analyzed the outcome of chromosome tethering to the microtubule cytoskeleton by quantifying "bouquets", a leptotene/zygotene chromosome configuration that arises from transient clustering of chromosome termini[39]. Staining with ACA antibodies to label the centromeric ends of mouse acrocentric chromosomes and SCP3 antibodies for staging revealed a significant reduction in telomere clustering in *Cep63^{T/T}* spermatocytes of juvenile mice compared to *WT* (Fig. 7b and 7c). Together our data suggests that in spermatocytes, CEP63 loss triggers cell death independently of p53, ATM or CHK2, primarily as a consequence of defective meiotic recombination, rather than mitotic spindle errors. Considering that CEP63 and CEP152 are physically separated from the chromosomes and can only be detected at centrosomes throughout prophase I (Fig. 6a), and that PCM organization is impaired in CEP63 deficient cells (Fig. 6e–h), we propose that these errors are likely caused by aberrant centrosomes that impair normal intranuclear chromosome movements (Fig. 7d).

Discussion

Cep63 deficient mice recapitulate two key aspects of human Seckel syndrome associated with *CEP63* mutations (SCKL6); growth retardation and microcephaly[5]. Our analysis suggests that the etiology of microcephaly in *Cep63^{T/T}* animals is partially distinct from that

reported for *Atr* or *Mcph1*. *Atr* deficiency causes more severe facial dysmorphia and runting than either *Mcph1* or *Cep63* deficiency[24, 44]. In addition, deletion of *p53* in *Atr* deficient animals exacerbates the neurodevelopmental phenotypes, whereas deletion of *p53* in *Cep63^T/T* mice rescued microcephaly (Fig. 3e–g). Rescue of microcephaly following p53 deletion has also been reported in other models with more severe centriole loss[25]. Microcephaly in *Mcph1* deficient mice has been linked to abrogated CHK1 recruitment to centrosomes and premature CDK1 activation that compromises the timing of division modes and self-renewal capacity of NPCs, resulting in their premature decline[27]. While we observed reduced neurosphere forming capacity of NPCs from *Cep63^T/T* embryos, we did not observe a progressive decline, as was reported in *Mcph1* mutants, suggesting that self-renewal defects are likely not the major cause of NPC depletion in *Cep63^T/T* mice (Supplementary Fig. 7). In addition, previous work has implicated CEP63 in CDK1 recruitment to centrosomes, arguing against a mechanism of premature centrosomal CDK1 activation[27, 45]. However, this issue will require further investigation since some of the CDK1 antibodies used for cytology cross-react with CEP152, that we, and others, have shown is dependent on CEP63 for centrosomal recruitment (Fig. 2a and 6a)[5, 22, 46–48].

We propose that defective CEP63/CEP152-dependent centriole duplication in *Cep63^T/T* mice leads to mitotic spindle defects in NPCs, including monopolar spindles and acentriolar spindle poles (Fig. 7d), as well as detachment and mislocalization of NPCs. This phenotype is very similar to what has been reported recently in mice lacking the essential centriole biogenesis factor SAS4[25] and is consistent with the previous proposition that centriole duplication defects in neural progenitor cells may be a major cause of human primary microcephaly[49]. Mitotic failure and subsequent G1 entry could result in polyploidy, that we have clearly observed in several *Cep63^T/T* cell types (Fig. 4b and Supplementary Fig. 2) and has also been reported in other systems[45]. However, an in depth FISH analysis in the developing cortex of SAS4 depleted animals, that have an even more dramatic centriole loss phenotype than *Cep63^T/T* mice, was unable to detect aneuploid cells, suggesting that stringent control mechanisms exist in the murine brain to prevent the accumulation of aneuploid cells[5, 45]. We believe that available data supports the idea that acentrosomal spindles and resulting mitotic spindle defects lead to mitotic delays that trigger p53-dependent cell death and promote microcephaly in *Cep63^T/T* animals[26, 50]. Such a mechanism would also be consistent with the inability of *Chk2* or *Atm* mutations to rescue the phenotype (Fig. 3f and g), the lack of extensive γH2AX staining (Fig. 3c), and the grossly normal DDR we have observed in cultured fibroblasts and during the immunological development of *Cep63^T/T* mice (Supplementary Fig. 2).

We have not obtained any evidence for defects in ATM/ATR related signaling in *Cep63^T/T* mice and the ATM/ATR dependent phosphorylation site identified in frog and chicken CEP63 is not conserved in the mammalian protein. However, as additional ATM/ATR consensus phosphorylation sites[51] exist in CEP63, it remains possible that CEP63 is a target of ATM/ATR or other damage induced modifications that affect its function after DNA damage. It also remains possible that the CEP63 paralogue, *Deup1*, provides some compensation, although we did not see evidence of increased *Deup1* mRNA levels in the brain (Fig. 1e)[52]. As CEP63 has been described to interact with the UVRAG protein that

influences DNA repair and autophagy, we cannot exclude that CEP63 has a role in the damage responses in tissues that we have not investigated or affects the DDR in a more subtle manner than can be detected by our assays[53].

Several mouse mutants in MCPH and Seckel genes exhibit both male and female subfertility or infertility[15, 54]. To our knowledge, this is the first example of male specific infertility associated with these disorders, but as only 3 female SCKL6 patients have been identified to date[5], we cannot confirm that this is the case in humans. The severity of the phenotype was surprising given the apparently normal DNA repair programs in the immune system (Supplementary Fig. 2), as well as the fertility and normal recombination observed in $Cep63^{T/T}$ females (Fig. 5g, Supplementary Fig. 3 and Supplementary Table 1). Centrioles can be detected in oocytes by TEM up to the pachytene stage[55] [56], but whether these represent bona fide centrosomes is unclear. We speculate that distinct requirements for the organization and function of the centrosome during meiotic prophase in males and females may explain the dramatic sex specificity we observe.

Meiotic recombination is the only DNA repair defect we have observed thus far in $Cep63^{T/T}$ mice or cell cultures. During prophase I, chromosomes are physically separated from the centrosome by the nuclear envelope and, in contrast to MCPH1 or ATR, we have seen no evidence for CEP63 nuclear translocation, although the limitations of the available immunoreagents preclude the definitive exclusion of this possibility (Fig. 6a)[15, 22, 57]. The major difference between homologous recombination in mitotic and meiotic cells is the use of the homologue, rather than the sister chromatid, as a template. As homologous chromosomes may be further apart than sister chromatids, global chromosome movements are likely to be required to facilitate timely homologue location and pairing. In addition, rapid chromosome movements have been proposed to dissociate non-homologous chromosome interactions[39, 58–61]. The centrosome is the major microtubule-organizing center (MTOC) and its composition and functions are defective in the absence of CEP63, potentially compromising the microtubule network and leading to impaired chromosome dynamics. This would be consistent with the fact that we have observed decreased telomere clustering, meiotic DNA repair defects and aberrant chromosome entanglements and fusions in CEP63 deficient mice (Fig. 7d). While chromosome positioning LINC complexes have also been implicated in neuronal pathology and infertility[20], defects in the interactions between the centrosome, microtubules and LINC complexes in $Cep63$ deficient animals could also play a role in other aspects of development.

In summary, our study has identified critical roles for CEP63 during brain development and suggests that increased p53-dependent cell death during embryogenesis could be the sole cause of microcephaly in some forms of Seckel syndrome and MCPH in human patients. In addition, it indicates that similar pathways are activated during neural development in response to acentrosomal and multicentrosomal spindle configurations[26, 28]. Future studies will be required to address the precise trigger(s) for p53 activation and to determine how generally this genetic dependency extends to other disorders resulting from centrosome defects. In addition, we have also uncovered an unexpected role for CEP63 in meiotic recombination, establishing the crosstalk between centrosome and recombination machinery as crucial for the fidelity of male gamete generation.

Methods

Generation and husbandry of mice

The generation of *Cep63* gene-trapped mice was described previously[22]. Mice lacking *p53* were purchased from Jackson Laboratories, *Chk2* deficient mice were obtained from Tak Mak[62] and Atm deficient mice from Anthony Winshaw-Boris[63]. All animals were maintained on a mixed 129/SvEv-C57BL/6 background in strict accordance with the European Community (86/609/EEC) guidelines at the animal facilities in the Barcelona Science Park (PCB). Protocols were approved by the Animal Care and Use Committee of the PCB (IACUC; CEEA-PCB) in accordance with applicable legislation (Law 5/1995/GC; Order 214/1997/GC; Law 1201/2005/SG). All efforts were made to minimize use and suffering.

Real-time quantitative PCR

Dissected tissue or primary MEFs were collected on ice, washed in PBS and frozen. Tissues were disrupted in lysis buffer by zirconium beads in a mechanical tissue disruptor (Precellys 24, Bertin technologies). RNA was isolated according to manufacturer recommendations (PureLink RNA mini kit, Ambion). 2 μg of RNA was used in a reverse-transcriptase reaction using a high-capacity RNA-to-cDNA kit (Applied Biosystems). Amplification of the cDNA was done with TaqMan master mix and specific probes for *Cep63, Anapc13, Plk4, Cep152* and *Deup1*. Probes for *B2m* and *ACTB* were used as housekeeping controls. Reactions were run on a 7900HT thermocycler (Applied Biosystems) and data plotted using SDS2.3 software. The $2^{-\Delta\Delta CT}$ method was used for the analysis of the amplification products.

Sperm counts

To determine sperm counts, cauda epididymis was dissected from 8–10 week old mice, cut with scissors in 5 places and incubated in 1 mL of warm PBS at 37°C for 10 min to let the sperm exit the tissue. After the incubation, sperm suspension was diluted 1:10 and manually counted under the microscope on the Neubauer glass slide counter.

Meiotic spreads

Testes from 8–10 week old mice (unless stated otherwise) were dissected, tunica was removed and tubules containing germ cells were disaggregated using a razor blade followed by passage through a p1000 tip in 1 mL of media (Dulbecco's modified Eagle medium supplemented with protease inhibitor cocktail, Roche 11873580001). The suspension was transferred to 5 mL of media and incubated for 5 min to precipitate larger pieces. Supernatant was distributed into 1 mL aliquots and centrifuged for 5 min at 7500 rpm. The pellet was suspended in 40 μL of hypotonic buffer containing 0.1 M sucrose supplemented with protease inhibitors and 20 μL of cell suspension was added to 70 μL of fixing solution (1% PFA with 0.1% Triton X-100) on the glass slide that was incubated in a humidified incubation chamber. After 2 hours, slides were rinsed with Ilfotol wetting agent (1:250 in water, Ilford) and processed immediately for immunofluorescence or stored at −80°C for later use.

Meiotic squashes

Spermatocyte squashes were performed as previously described[64, 65]. In brief, tubules from 10 days or 8–10 week old mice (unless stated otherwise) were placed directly in fixative solution (2% formaldehyde, 0.05% Triton-X 100 in PBS) for 10 minutes. To release spermatocytes from tubules, a small aliquot of the tubules was minced with tweezers on a glass slide pre-treated with poly-L lysine. Cells were covered with a coverslip and gently squashed by applying pressure with the thumb. The slide was snap-frozen in liquid nitrogen, the coverslip was removed and the slide was immediately processed for immunofluorescence. Alternatively, tubules were minced without fixation, squashed and frozen in liquid nitrogen. After removal of the coverslip, slides were fixed in ice-cold 95% ethanol for 10 min followed by 4% formaldehyde for 7min (the latter protocol improves centrosome morphology).

Immunofluorescence analysis

Slides with spermatocytes were washed in blocking solution (1% BSA, 0.05% Tween-20 in PBS) for 30 minutes and then incubated with primary antibody overnight in a humidified chamber at 4°C. Slides were washed multiple times in blocking solution and incubated with complementary Alexa Fluor conjugated secondary antibody for 2 hours at RT. Slides were extensively washed with blocking solution and in the last washing step DAPI was used as a counter stain (unless stated otherwise). Slides were then mounted using Prolong Gold antifade reagent (Life Technologies). For double antigen staining, two primary antibodies of different origin were combined together in an overnight incubation. For triple antigen staining, two primary antibodies of different origin were combined together in the first overnight incubation, then washed and incubated with complementary secondary antibodies. Third antigen staining (mouse SCP3 in squashes, mouse γH2Ax in spreads) was incubated overnight and then visualized with Alexa Fluor 350 conjugated anti-mouse secondary antibody (Life Technologies).

Immunohistochemistry

Freshly dissected testes and ovaries of the indicated age were fixed in Bouin's solution (Electron Microscopy Sciences) or in 10% neutral buffered formalin (5 days old testes) and embedded in paraffin using standard procedures. Sections were cut at 5 μm thickness and stained with hematoxylin and eosin (H&E, testes) or hematoxylin and Periodic acid/Schiff reagent (PAS, Sigma-Aldrich, testes and ovaries). 5 days old testes were immuno-labeled with WT1 antibody (Novus Biologicals) and counterstained with hematoxylin. P60 brains were dissected from animals and fixed overnight in 10% neutral buffered formalin (Sigma), embedded in paraffin using standard procedures and stained with H&E. For brain cryosections, E14.5 mouse heads were fixed with 4% PFA for 48h, cryoprotected in 30% sucrose and frozen in OCT at −80°C. P2 animals were anesthetized with ice and perfused intracardially with PBS followed by 4% PFA. Brains were removed, post-fixed with 4% PFA overnight, cryoprotected in 30% sucrose and frozen in OCT at −80°C. Cryosections were cut at 10 μm thickness and fixed to frosted glass slides by incubation for 20 min in ice-cold acetone at −20°C. Slides were then washed several times in PBS followed with washing in PBS-T (0.3% Triton X-100 in PBS) and blocked with 5% goat serum in PBS-T

for 60 min. Slides were incubated overnight at 4°C with primary antibody, next day washed several times in PBS-T and stained with Alexa-Fluor conjugated complementary secondary antibody for 60 min at RT. After final washing, DNA was counterstained with Hoechst 33342. For SOX2 and TBR2 staining, an antigen retrieval procedure was performed before the blocking step by incubating tissue sections in citrate-based buffer for 5min in a microwave pressure cooker at 70% power. For TUNEL staining, Bouin's solution fixed paraffin embedded sections of 8–10 weeks old mice testes or cryosections of 4% PFA fixed mouse embryonic brains were labeled with In SituCell Death Detection Kit (TUNEL) according to the manufacturer's instructions (Roche, 11684795910). For colorimetric visualization, sections were incubated with cleaved-caspase 3 antibody overnight at room temperature after quenching endogenous peroxidase using 0.6% H_2O_2 (vol/vol) in methanol. Slides were washed with PBS three times, followed by incubation with biotinylated secondary antibody and avidin-biotin complex (Vectastain Elite kit, Vector Labs). Immunoreactive signals were visualized with the VIP substrate kit (Vector Labs) using the manufacturer's protocol. Sections were counterstained with 0.1% methyl green (wt/vol), dehydrated, and mounted in DPX (Fluka).

Antibodies

Primary antibodies are listed in Supplementary Table 2. Secondary antibodies used: FITC- and Cy3-conjugated secondary antibodies (Jackson Immunologicals), Alexa Fluor 350-, 488- and 568-conjugated goat anti-mouse, Alexa Fluor 488- and 568-conjugated goat anti-rabbit, Alexa Fluor 488-conjugated goat anti-guinea pig and Alexa Fluor 568-conjugated anti-human antibodies (Life technologies).

Microscopy

Brain histological sections were imaged with a macroscope (Olympus MVX10) and neocortical thickness was measured in comparative sections from the pia to the white matter. At P2 cortical thickness was measured in motor, somatosensory and visual cortex (2.31mm, 3.75mmand 4.23mm, respectively according to reference[66]) and at P60 in motor and visual cortex (Bregma: 1.42 and −2.70, respectively). Fluorescent images were acquired with an Orca AG camera (Hamamatsu) mounted on a Leica DMI6000B microscope equipped with 1.4 NA 63× and 100× oil immersion objectives. AF6000 software (Leica) was used for image acquisition and deconvolution of z-stack images (distance between z-slices was 0.2 μm). Coronal/sagittal serial brain sections from embryos at E14.5 from multiple animals per genotype were analyzed in each experiment (details in figure legends). For cell counts in the cortex all cells from the ventricular surface to the pial surface were counted and normalized with the area selected (mm^2). Additional image processing and maximum intensity z-projections were done in ImageJ software. Mitotic figure classification was done using apical mitosis within cortical sections imaged with a Leica TCS SP5 laser scanning spectral confocal microscope set up on a Leica DMI600 inverted microscope. Confocal Z-stacks were acquired with 0.2 μm of step size and using laser parameters which minimized the presence of saturated pixels. γ-tubulin distribution in mitotic centrosomes was calculated assigning centrosomes to the "2 bright poles" category when both γ-tubulin signals fell within the 40–60% of distribution of their bright/dim ratio and "1 dim or absent pole"

category if one of the γ-tubulin signals fell within a 60–100% distribution of bright/dim ratio.

Transmission electron microscopy

Testes of mature mice were dissected and fixed for transmission electron microscopy (TEM) analysis as previously described[67]. Briefly, testes were pre-fixed in cacodylate-buffered glutaraldehyde and post fixed in buffered OsO4 followed by Renlam® M-1 resin (Serva, Heidelberg, Germany). Ultrathin sections were analyzed in a Tecnai12 BioTwin TEM (FEI, Eindhoven, NL) and imaged with a CCD camera (SIS MegaView3, Surface Imaging Systems, Herzogenrath, Germany) and the Analysis Imaging Interface. Contrast and brightness of images were further adjusted using Adobe Photoshop CS.

Statistics

All graphics with error bars are presented as average + s.d. (except in Fig. 6c where only average bar is shown and Fig. 1a-1b and 5b–c where median with 1st and 3rd quartile of the box plot is shown. To determine statistical significance between samples, unpaired two-way Wilcoxon rank-sum test was used on samples with 8 or more read-outs (Fig. 1b, 4b, 5b–c and 5g), while in cases with < 8 read-outs, unpaired two-way Student t-test was used (Fig. 1a, 1g, 2d, 2h, 3b, 3d, 3g, 3h, 3j, 4a, 4d, 4f and 7b). Log-rank test was used for Kaplan-Meier comparison (Fig. 1h). Statistical calculations and generation of graphics were performed in Excel, R console, Graphpad Prism or Mstat (n.s. = non significant, * $p < 0.05$, ** $p < 0.01$, *** $p < 0.001$).

Supplementary Material

Refer to Web version on PubMed Central for supplementary material.

Acknowledgements

References

1. Qvist P, et al. CtIP Mutations Cause Seckel and Jawad Syndromes. PLoS Genet. 2011; 7:e1002310. [PubMed: 21998596]

2. Griffith E, et al. Mutations in pericentrin cause Seckel syndrome with defective ATR-dependent DNA damage signaling. Nat Genet. 2008; 40:232–236. [PubMed: 18157127]

3. O'Driscoll M, Ruiz-Perez VL, Woods CG, Jeggo PA, Goodship JA. A splicing mutation affecting expression of ataxia-telangiectasia and Rad3-related protein (ATR) results in Seckel syndrome. Nat Genet. 2003; 33:497–501. [PubMed: 12640452]

4. Thornton GK, Woods CG. Primary microcephaly: do all roads lead to Rome? Trends Genet. 2009; 25:501–510. [PubMed: 19850369]

5. Sir JH, et al. A primary microcephaly protein complex forms a ring around parental centrioles. Nat Genet. 2011; 43:1147–1153. [PubMed: 21983783]

6. Klingseisen A, Jackson AP. Mechanisms and pathways of growth failure in primordial dwarfism. Genes Dev. 2011; 25:2011–2024. [PubMed: 21979914]

7. Guernsey DL, et al. Mutations in centrosomal protein CEP152 in primary microcephaly families linked to MCPH4. Am J Hum Genet. 2010; 87:40–51. [PubMed: 20598275]

8. Mahmood S, Ahmad W, Hassan MJ. Autosomal Recessive Primary Microcephaly (MCPH): clinical manifestations, genetic heterogeneity and mutation continuum. Orphanet J Rare Dis. 2011; 6:39. [PubMed: 21668957]

9. Kalay E, et al. CEP152 is a genome maintenance protein disrupted in Seckel syndrome. Nat Genet. 2011; 43:23–26. [PubMed: 21131973]

10. Kumar A, Girimaji SC, Duvvari MR, Blanton SH. Mutations in STIL, encoding a pericentriolar and centrosomal protein, cause primary microcephaly. Am J Hum Genet. 2009; 84:286–290. [PubMed: 19215732]

11. Bond J, et al. A centrosomal mechanism involving CDK5RAP2 and CENPJ controls brain size. Nat Genet. 2005; 37:353–355. [PubMed: 15793586]

12. Nicholas AK, et al. WDR62 is associated with the spindle pole and is mutated in human microcephaly. Nat Genet. 2010; 42:1010–1014. [PubMed: 20890279]

13. Lancaster MA, et al. Cerebral organoids model human brain development and microcephaly. Nature. 2013; 501:373–379. [PubMed: 23995685]

14. Jeffers LJ, Coull BJ, Stack SJ, Morrison CG. Distinct BRCT domains in Mcph1/Brit1 mediate ionizing radiation-induced focus formation and centrosomal localization. Oncogene. 2008; 27:139–144. [PubMed: 17599047]

15. Liang Y, et al. BRIT1/MCPH1 is essential for mitotic and meiotic recombination DNA repair and maintaining genomic stability in mice. PLoS Genet. 2010; 6:e1000826. [PubMed: 20107607]

16. Alderton GK, et al. Regulation of mitotic entry by microcephalin and its overlap with ATR signalling. Nat Cell Biol. 2006; 8:725–733. [PubMed: 16783362]

17. Kramer A, et al. Centrosome-associated Chk1 prevents premature activation of cyclin-B-Cdk1 kinase. Nat Cell Biol. 2004; 6:884–891. [PubMed: 15311285]

18. Tibelius A, et al. Microcephalin and pericentrin regulate mitotic entry via centrosome-associated Chk1. J Cell Biol. 2009; 185:1149–1157. [PubMed: 19546241]

19. Gillies TE, Cabernard C. Cell division orientation in animals. Curr Biol. 2011; 21:R599–R609. [PubMed: 21820628]

20. Zhang X, et al. SUN1/2 and Syne/Nesprin-1/2 complexes connect centrosome to the nucleus during neurogenesis and neuronal migration in mice. Neuron. 2009; 64:173–187. [PubMed: 19874786]

21. Smith E, et al. An ATM- and ATR-dependent checkpoint inactivates spindle assembly by targeting CEP63. Nat Cell Biol. 2009; 11:278–285. [PubMed: 19182792]

22. Brown NJ, Marjanovic M, Luders J, Stracker TH, Costanzo V. Cep63 and cep152 cooperate to ensure centriole duplication. PLoS One. 2013; 8:e69986. [PubMed: 23936128]

23. Lukinavicius G, et al. Selective chemical crosslinking reveals a Cep57-Cep63-Cep152 centrosomal complex. Curr Biol. 2013; 23:265–270. [PubMed: 23333316]

24. Murga M, et al. A mouse model of ATR-Seckel shows embryonic replicative stress and accelerated aging. Nat Genet. 2009; 41:891–898. [PubMed: 19620979]

25. Insolera R, Bazzi H, Shao W, Anderson KV, Shi SH. Cortical neurogenesis in the absence of centrioles. Nature neuroscience. 2014; 17:1528–1535. [PubMed: 25282615]

26. Bazzi H, Anderson KV. Acentriolar mitosis activates a p53-dependent apoptosis pathway in the mouse embryo. Proc Natl Acad Sci U S A. 2014; 111:E1491–E1500. [PubMed: 24706806]

27. Gruber R, et al. MCPH1 regulates the neuroprogenitor division mode by coupling the centrosomal cycle with mitotic entry through the Chk1-Cdc25 pathway. Nat Cell Biol. 2011; 13:1325–1334. [PubMed: 21947081]

28. Marthiens V, et al. Centrosome amplification causes microcephaly. Nat Cell Biol. 2013; 15:731–740. [PubMed: 23666084]

29. Carvajal LA, Manfredi JJ. Another fork in the road--life or death decisions by the tumour suppressor p53. EMBO Rep. 2013; 14:414–421. [PubMed: 23588418]

30. Frappart PO, et al. An essential function for NBS1 in the prevention of ataxia and cerebellar defects. Nat Med. 2005; 11:538–544. [PubMed: 15821748]

31. Novorol C, et al. Microcephaly models in the developing zebrafish retinal neuroepithelium point to an underlying defect in metaphase progression. Open Biol. 2013; 3:130065. [PubMed: 24153002]

32. Hutton SR, Pevny LH. SOX2 expression levels distinguish between neural progenitor populations of the developing dorsal telencephalon. Dev Biol. 2011; 352:40–47. [PubMed: 21256837]

33. Stracker TH, Roig I, Knobel PA, Marjanovic M. The ATM signaling network in development and disease. Frontiers in genetics. 2013; 4:37. [PubMed: 23532176]

34. Baudat F, Manova K, Yuen JP, Jasin M, Keeney S. Chromosome synapsis defects and sexually dimorphic meiotic progression in mice lacking Spo11. Mol Cell. 2000; 6:989–998. [PubMed: 11106739]

35. Romanienko PJ, Camerini-Otero RD. The mouse Spo11 gene is required for meiotic chromosome synapsis. Mol Cell. 2000; 6:975–987. [PubMed: 11106738]

36. Horn HF. LINC complex proteins in development and disease. Current topics in developmental biology. 2014; 109:287–321. [PubMed: 24947240]

37. Cizmecioglu O, et al. Cep152 acts as a scaffold for recruitment of Plk4 and CPAP to the centrosome. J Cell Biol. 2010; 191:731–739. [PubMed: 21059844]

38. Sato A, et al. Cytoskeletal forces span the nuclear envelope to coordinate meiotic chromosome pairing and synapsis. Cell. 2009; 139:907–919. [PubMed: 19913287]

39. Klutstein M, Cooper JP. The Chromosomal Courtship Dance-homolog pairing in early meiosis. Curr Opin Cell Biol. 2014; 26:123–131. [PubMed: 24529254]

40. Shibuya H, Ishiguro K, Watanabe Y. The TRF1-binding protein TERB1 promotes chromosome movement and telomere rigidity in meiosis. Nat Cell Biol. 2014; 16:145–156. [PubMed: 24413433]

41. Rattner JB. Observations of centriole formation in male meiosis. J Cell Biol. 1972; 54:20–29. [PubMed: 5038873]

42. Link J, et al. Analysis of meiosis in SUN1 deficient mice reveals a distinct role of SUN2 in mammalian meiotic LINC complex formation and function. PLoS Genet. 2014; 10:e1004099. [PubMed: 24586178]

43. Horn HF, et al. A mammalian KASH domain protein coupling meiotic chromosomes to the cytoskeleton. J Cell Biol. 2013; 202:1023–1039. [PubMed: 24062341]

44. Trimborn M, et al. Establishment of a mouse model with misregulated chromosome condensation due to defective Mcph1 function. PLoS One. 2010; 5:e9242. [PubMed: 20169082]

45. Loffler H, et al. Cep63 recruits Cdk1 to the centrosome: implications for regulation of mitotic entry, centrosome amplification, and genome maintenance. Cancer Res. 2011; 71:2129–2139. [PubMed: 21406398]

46. Lukinavicius G, Lavogina D, Gonczy P, Johnsson K. Commercial Cdk1 antibodies recognize the centrosomal protein Cep152. Biotechniques. 2013; 55:111–114. [PubMed: 24137814]

47. Alsara M, Loffler H, Fechter A, Bartek J, Kramer A. Cep63 Recruits Cdk1 to the Centrosome-Letter. Cancer Res. 2015

48. Alsara M, Loffler H, Fechter A, Bartek J, Kramer A. Cep63 recruits cdk1 to the centrosome-letter. Cancer Res. 2015; 75:777–778. [PubMed: 25643699]

49. Lin YC, et al. Human microcephaly protein CEP135 binds to hSAS-6 and CPAP, and is required for centriole assembly. EMBO J. 2013; 32:1141–1154. [PubMed: 23511974]

50. Andreassen PR, Lohez OD, Lacroix FB, Margolis RL. Tetraploid state induces p53-dependent arrest of nontransformed mammalian cells in G1. Mol Biol Cell. 2001; 12:1315–1328. [PubMed: 11359924]

51. Hornbeck PV, et al. PhosphoSitePlus: a comprehensive resource for investigating the structure and function of experimentally determined post-translational modifications in man and mouse. Nucleic Acids Res. 2012; 40:D261–D270. [PubMed: 22135298]

52. Zhao H, et al. The Cep63 paralogue Deup1 enables massive de novo centriole biogenesis for vertebrate multiciliogenesis. Nat Cell Biol. 2013; 15:1434–1444. [PubMed: 24240477]

53. Zhao Z, et al. A dual role for UVRAG in maintaining chromosomal stability independent of autophagy. Dev Cell. 2012; 22:1001–1016. [PubMed: 22542840]

54. Pulvers JN, et al. Mutations in mouse Aspm (abnormal spindle-like microcephaly associated) cause not only microcephaly but also major defects in the germline. Proc Natl Acad Sci U S A. 2010; 107:16595–16600. [PubMed: 20823249]

55. Szollosi D, Calarco P, Donahue RP. Absence of centrioles in the first and second meiotic spindles of mouse oocytes. J Cell Sci. 1972; 11:521–541. [PubMed: 5076360]

56. Manandhar G, Schatten H, Sutovsky P. Centrosome reduction during gametogenesis and its significance. Biol Reprod. 2005; 72:2–13. [PubMed: 15385423]

57. Cimprich KA, Cortez D. ATR: an essential regulator of genome integrity. Nat Rev Mol Cell Biol. 2008; 9:616–627. [PubMed: 18594563]

58. Koszul R, Kleckner N. Dynamic chromosome movements during meiosis: a way to eliminate unwanted connections? Trends Cell Biol. 2009; 19:716–724. [PubMed: 19854056]

59. Koszul R, Kim KP, Prentiss M, Kleckner N, Kameoka S. Meiotic chromosomes move by linkage to dynamic actin cables with transduction of force through the nuclear envelope. Cell. 2008; 133:1188–1201. [PubMed: 18585353]

60. Wanat JJ, et al. Csm4, in collaboration with Ndj1, mediates telomere-led chromosome dynamics and recombination during yeast meiosis. PLoS Genet. 2008; 4:e1000188. [PubMed: 18818741]

61. Zickler D. From early homologue recognition to synaptonemal complex formation. Chromosoma. 2006; 115:158–174. [PubMed: 16570189]

62. Hirao A, et al. Chk2 is a tumor suppressor that regulates apoptosis in both an ataxia telangiectasia mutated (ATM)-dependent and an ATM-independent manner. Mol Cell Biol. 2002; 22:6521–6532. [PubMed: 12192050]

63. Barlow C, et al. Atm-deficient mice: a paradigm of ataxia telangiectasia. Cell. 1996; 86:159–171. [PubMed: 8689683]

64. Page J, Suja JA, Santos JL, Rufas JS. Squash procedure for protein immunolocalization in meiotic cells. Chromosome Res. 1998; 6:639–642. [PubMed: 10099877]

65. Sitaram P, Hainline SG, Lee LA. Cytological analysis of spermatogenesis: live and fixed preparations of Drosophila testes. Journal of visualized experiments : JoVE. 2014:e51058. [PubMed: 24473184]

66. Paxinos, G. Atlas of the Developing Mouse Brain: At E17.5, PO. Academic Press; 2007.

67. Avasthi P, et al. Germline deletion of Cetn1 causes infertility in male mice. J Cell Sci. 2013; 126:3204–3213. [PubMed: 23641067]
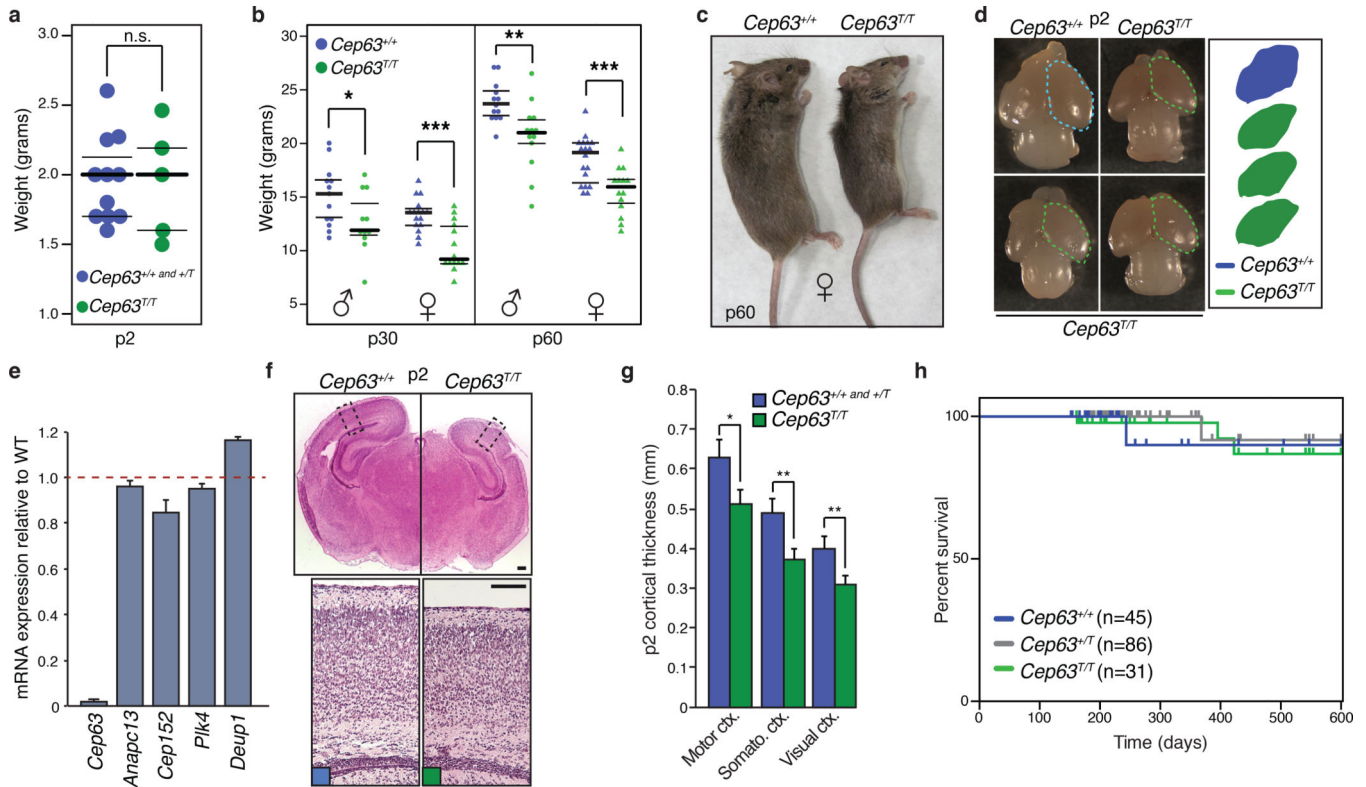
Figure 1. *Cep63* deficiency leads to growth defects and microcephaly
(**a**) Weights of newborn mice (p2) of the indicated genotype (*Cep63*[+/+, +/T] n = 11, *Cep63*[T/T] n = 5 pups). (**b**) Weight of p30 and p60 mice of the indicated sex and genotype (n = 13, 11, 16, 14, 13, 13, 18, 14 animals, respectively). (**c**) Examples of female littermate *Cep63*^{+/+} and *Cep63*[T/T] mice at p60. (**d**) Examples of p2 dissected brains of the indicated genotype with the relative cerebral cortex area compared. (**e**) Quantitative real-time PCR of the indicated genes using cDNA prepared from the cortex of p2 animals. Levels of mRNA expression relative to *WT* littermates is graphed using *B2M* and *ACTB* as a reference. (n=3 animals per genotype). (**f**) H&E stained coronal sections of *Cep63*^{+/+} and *Cep63*[T/T] cortices from p2 animals with approximate area of higher magnification indicated (top panels). Higher magnification panels of the motor cortex stained with H&E (bottom panels, scale bar = 0.2 mm). (**g**) Quantification of p2 cortical thickness from the indicated genotypes and area (2 hemispheres per brain section were averaged, n = 3 animals is graphed). (**h**) Kaplan-Meier curve of mouse survival. No significant differences (Log-rank test) were observed over 600 days. The number of animals per genotype is indicated. In panels 1a and 1b, the median (thick line) with the 1st and 3rd quartiles of the boxplot (thin lines) are indicated. In 1e and 1g graphics with error bars represent the average plus standard deviation. Asterisks denote statistical significance (n.s.= not significant, * = p-value <0.05, ** = p-value < 0.01, *** = p-value < 0.001) determined by the unpaired two-way Student's T-test (1a, 1g) or the unpaired two-way Wilcoxon rank sum test (1b).
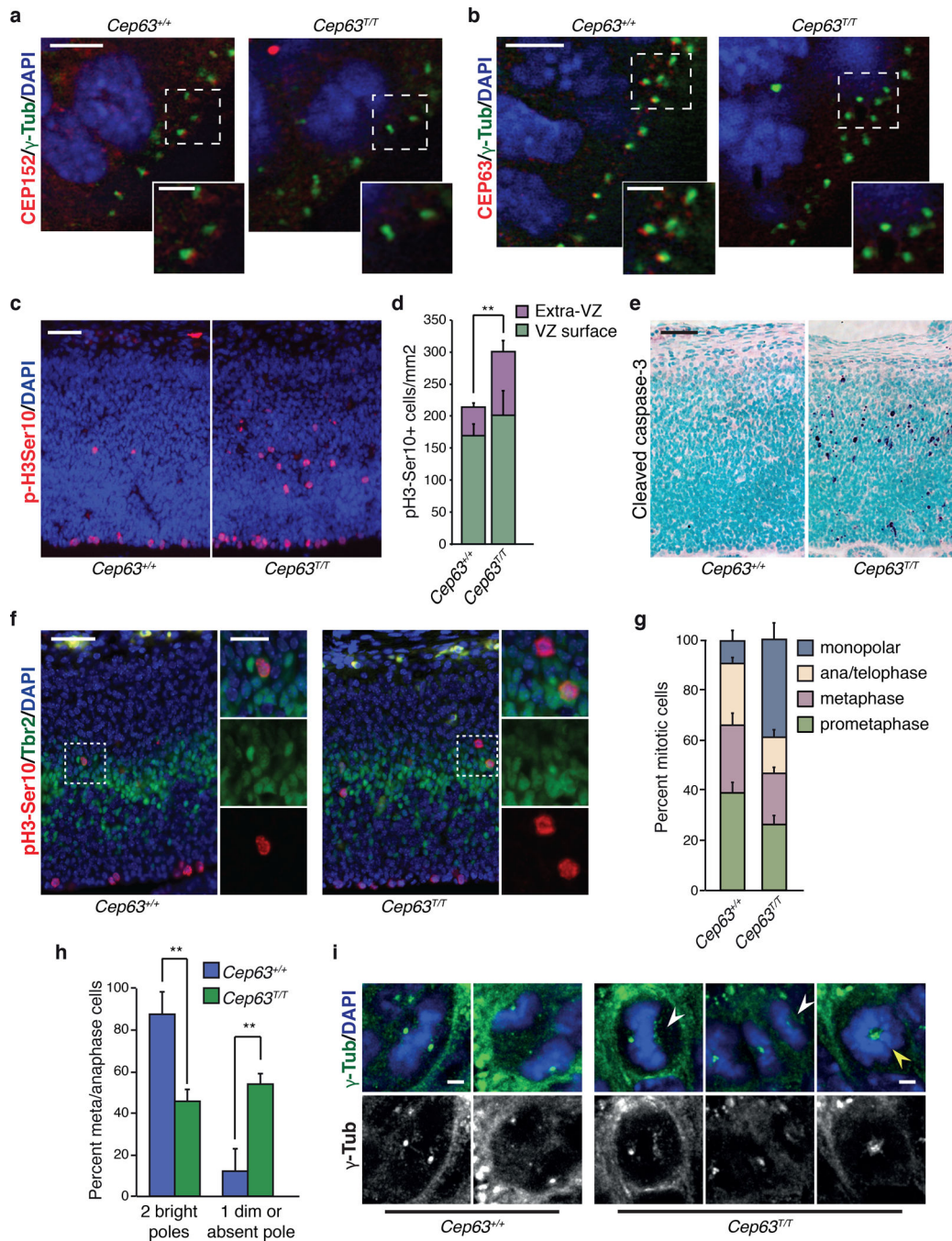
Figure 2. Impaired CEP152 localization and mitotic defects in *Cep63* deficient brains
(**a**) CEP152 is detectable at centrosomes, marked by γ-tubulin, in the cortex of WT (left panel) but not *Cep63*[T/T] (right panel) E14.5 embryos (scale bars represent 5 μm (left) and 2 μm (right)). (**b**) CEP63 is detectable at centrosomes, marked by γ-tubulin, in the cortex of WT (left panel) but not *Cep63*[T/T] E14.5 embryos (right panel). (scale bars represent 5 μm (left) and 2μm (right)). (**c**) Increased number and defective localization of mitotic cells (positive for p-H3Ser10) in the E14.5 cortex of *Cep63*[T/T] embryos (right panel) compared to WT (left panel). (scale bar = 50 μm). (**d**) Quantification of VZ surface and extra-VZ p-

H3Ser10 positive mitoses in the indicated genotype (n = 5 and 3 animals per genotype, respectively). (**e**) Increased cleaved caspase-3 staining indicates increased cell death in the cortex of *Cep63^(T/T)* embryos at E14.5 (right panel) compared to WT (left panel). (scale bar = 50 μm). (**f**) Some misplaced mitotic cells in the *Cep63^(T/T)* cortex are intermediate progenitors (IPs) identified by positivity for Tbr2 (scale bars represent 50 μm (left) and 20 μm (right)). (**g**) Scoring of mitotic configurations in the E14.5 VZ. Categories and genotypes are indicated (n = 3 animals per genotype used, 102 *Cep63^(+/+)* and 150 *Cep63^(T/T)* cells scored). (**h**) Scoring of γ-tubulin foci in metaphase and anaphase cells in VZ of E14.5 brain cortex. Mitotic cells were identified by staining sections with DAPI (DNA) and γ-tubulin (centrosome) and scored by morphology and γ-tubulin spot numbers (n = 3 animals per genotype used, 64 *Cep63^(+/+)* and 62 *Cep63^(T/T)* cells scored). (**i**) Example images of acentrosomal (white arrowheads) and monopolar (yellow arrowhead) mitoses in *Cep63^(T/T)* embryos (scale bar = 2 μm). All graphics with error bars are presented as the average plus standard deviation. Asterisks denote statistical significance (n.s.= not significant, * = p-value <0.05, ** = p-value < 0.01, *** = p-value < 0.001) determined by the unpaired two-way Student's T-test (2d and 2h).
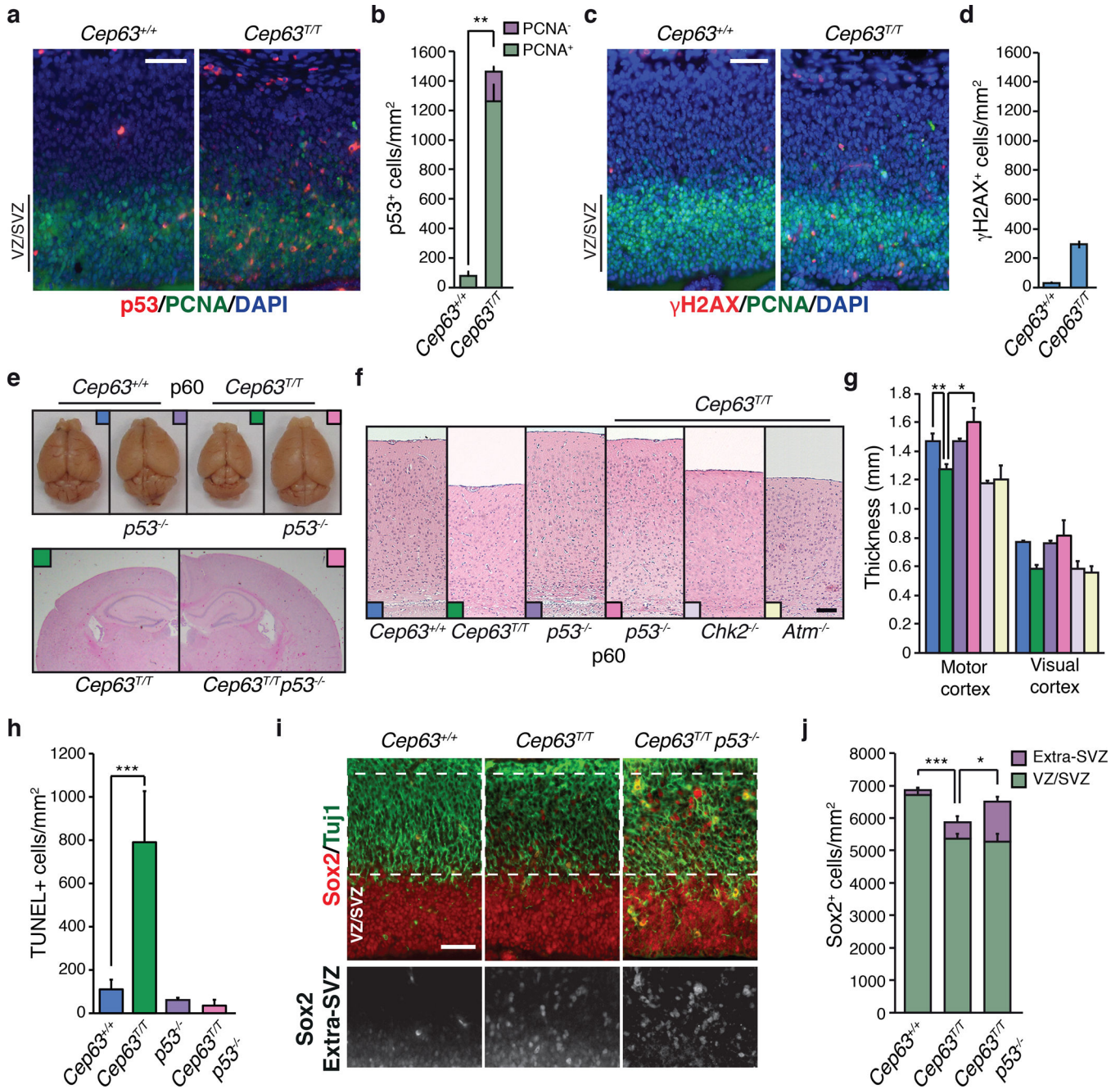
Figure 3. p53-dependent attrition of neural progenitors in *Cep63* deficient embryos
(**a**) Strong induction of p53 in the cortex of *Cep63*[T/T] embryos compared to *WT* at E14.5
(scale bar = 50 μm). (**b**) Scoring of p53-positive cells in **a** (n = 2 animals per genotype). (**c**)
Slightly increased levels of γH2AX can be visualized in the E14.5 cortex of *Cep63*[T/T]
embryos compared to *WT* (scale bar = 50 μm). (**d**) Quantification of γH2AX-positive cells in
c (n = 1 animal per genotype). (**e**) Dissected p60 brains (upper panel) and representative
coronal sections from *Cep63*[T/T] and *Cep63*[T/T]*p53*^{−/−} mice (lower panel). (**f**) Representative
examples illustrating relative p60 motor cortex thickness in mice of the indicated genotype
(scale bar = 0.2 mm). (**g**) Measurement of cortex thickness from sections of the motor or

visual cortex with colors corresponding to genotypes in panel f (n = 3, 3, 2, 3, 2, 2 animals used per genotype, respectively). (**h**) Quantification of TUNEL staining (n = 6, 10, 4, 4 sections per animal were scored, sections from 2, 3, 1, 1 animals per genotype were used, respectively). (**i**) Misplacement of neural/stem cell progenitors (Sox2 positive) in $Cep63^{T/T}$ and $Cep63^{T/T}p53^{-/-}$ animals (scale bar = 50 μm). (**j**) Rescue of misplaced progenitors in $Cep63^{T/T}p53^{-/-}$ animals compared to $Cep63^{T/T}$ (n = 5, 3 and 3 animals per genotype, respectively). All graphics with error bars are presented as the average plus standard deviation. Asterisks denote statistical significance (n.s.= not significant, * = p-value <0.05, ** = p-value < 0.01, *** = p-value < 0.001) determined by the unpaired two-way Student's T-test (3b, 3g, 3h and 3j).
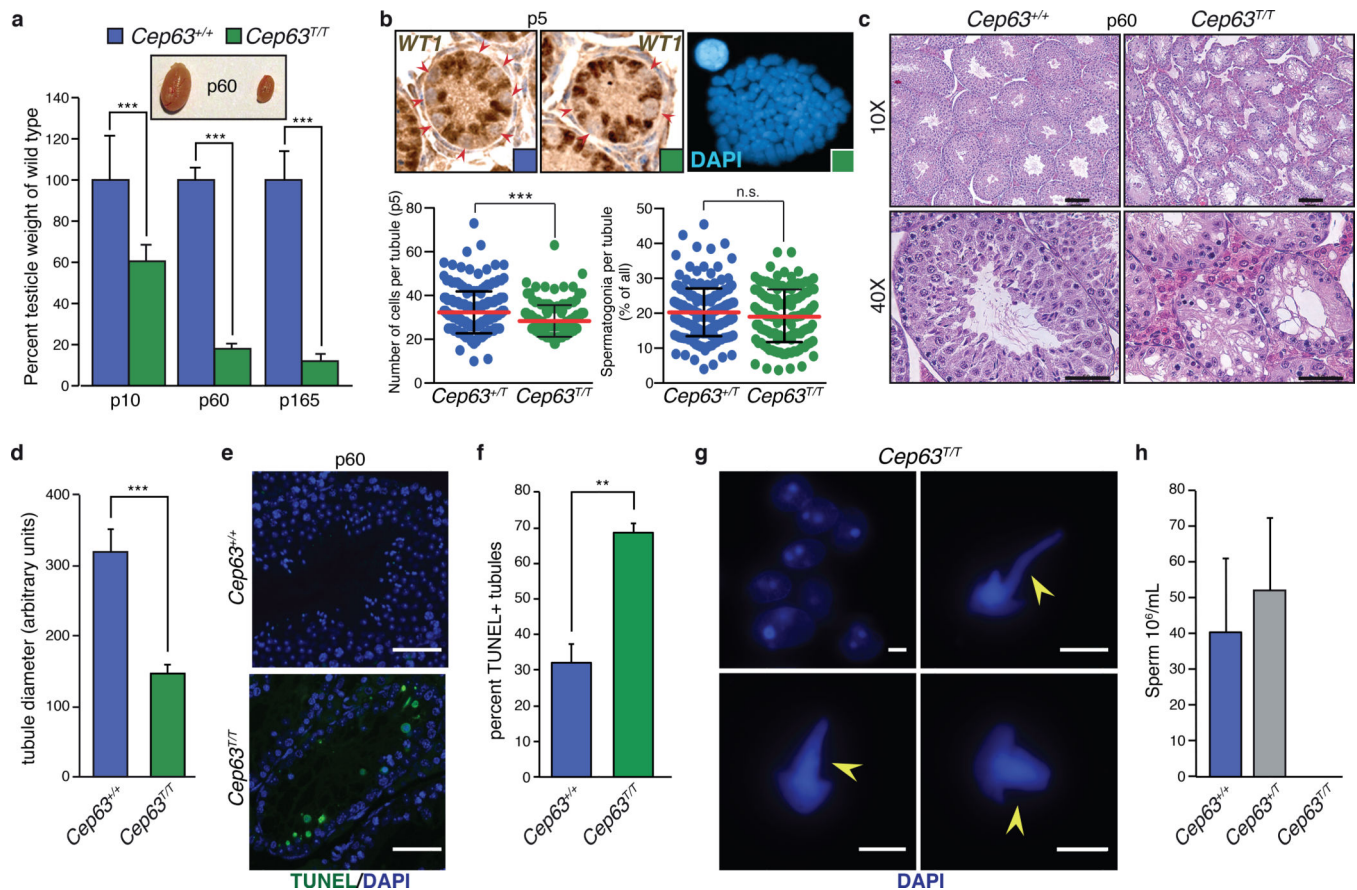
Figure 4. Infertility and severe defects in testes development in *Cep63^{T/T}* mice

(**a**) Comparison of testicle weight to WT littermates at p10, p60 and p165. Examples of dissected p60 testes are shown (n = 4, 3, 8, 8, 2 and 4 animals, respectively). (**b**) Testes sections from p5 animals were stained with antibody against WT1 (upper panels) and WT1 negative cells (spermatagonia, red arrows) were scored and plotted (lower panels). Reduced cell numbers in p5 tubules (bottom left panel) but proportionally similar numbers of spermatagonia (bottom right panel) were observed (results are combined from 4 *Cep63^{+/T}* and 3 *Cep63^{T/T}* animals. For *Cep63^{+/T}* n = 201 and *Cep63^{T/T}* n = 143 tubules scored). Individual values are shown in a scatterplot with the average (red line) and standard deviation (black lines) indicated. Tetraploidy was observed in some spermatagonia from *Cep63^{T/T}* animals (upper right panel). (**c**) H&E staining of testes sections from p60 mice showing relative size and condition of tubules (scale bar = 100 μm in 10X panels and 50 μm in 40X panels). (**d**) Quantification of tubule size in the indicated genotypes (2 animals per genotype, n = 6 tubules per genotype measured). (**e**) Examples of TUNEL staining (scale bar = 50 μm). (**f**) Quantification of TUNEL positive tubules (n = 3 animals per genotype used, 279 *Cep63^{+/+}* and 266 *Cep63^{T/T}* tubules scored). (**g**) Examples of aberrant spermatids from *Cep63^{T/T}* testes squashes. DAPI stained tails are indicated with yellow arrows (scale bar = 5 μm). (**h**) Sperm counts from mice of the indicated genotypes (n = 4, 2 and 4 animals per genotype, respectively). All graphs with error bars are presented as the average plus standard deviation. Asterisks denote statistical significance (n.s.= not significant, * = p-value <0.05,

** = p-value < 0.01, *** = p-value < 0.001) determined by the unpaired two-way Student's T-test (4a, 4d, 4f) or the unpaired two-way Wilcoxon rank sum test (4b).
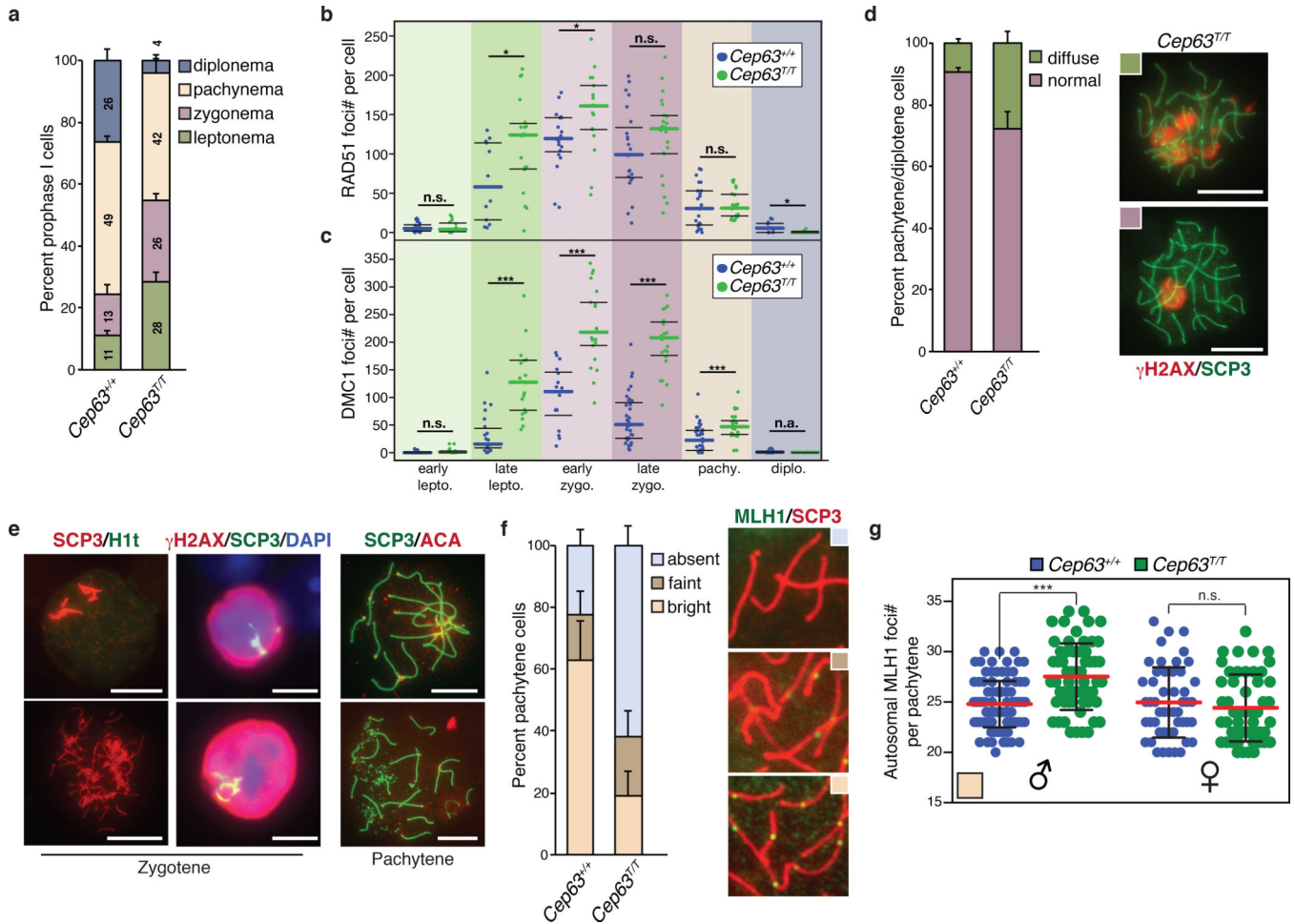
Figure 5. Impaired meiotic progression in *Cep63^{T/T}* mice

(**a**) Quantification of prophase I stages in meiotic cells of the indicated genotype based on co-staining of SCP1 and SCP3 (n = 3 animals per genotype used, 289 *Cep63^{+/+}* and 301 *Cep63^{T/T}* cells scored). Quantification of RAD51 (**b**) and DMC1 (**c**) foci in the indicated stages of prophase I (assessed by SCP3 staining) from the indicated genotypes (*Cep63^{+/+}* n = 112 and 157, *Cep63^{T/T}* n = 122 and 108 cells scored, respectively). (**d**) Quantification of γH2AX staining patterns in pachytene and diplotene cells (n = 3 animals per genotype used, 124 *Cep63^{+/+}* and 97 *Cep63^{T/T}* cells scored), example spermatocyte spreads shown (scale bar = 10 μm). (**e**) Examples of aberrant SC structures observed in zygotene and pachytene spermatocytes from *Cep63^{T/T}* spreads (scale bar = 10 μm). (**f**) Quantification of crossover formation using MLH1 staining. Reduced numbers of *Cep63^{T/T}* pachytene cells have visible MLH1 foci (n = 3 animals per genotype used, 84 and 59 cells scored respectively). Examples of categories scored are shown right panels. (**g**) Scoring of MLH1 foci in pachytene cells with visible MLH1 foci. In the low percentage of *Cep63^{T/T}* males that have visible foci, there is a significant increase in foci number (n=101 and 135 cells scored). MLH1 foci in females is comparable regardless of genotype (*Cep63^{+/+ or +/−}* n = 2(M)/2(F) and *Cep63^{T/T}* n = 3(M)/2(F) animals). Individual values are shown in a scatterplot with the average (red line) and standard deviation (black lines) indicated. All graphs with error bars

are presented as the average plus standard deviation. Asterisks denote statistical significance (n.s.= not significant, * = p-value <0.05, ** = p-value < 0.01, *** = p-value < 0.001) determined by the unpaired two-way Wilcoxon rank sum test (4g).

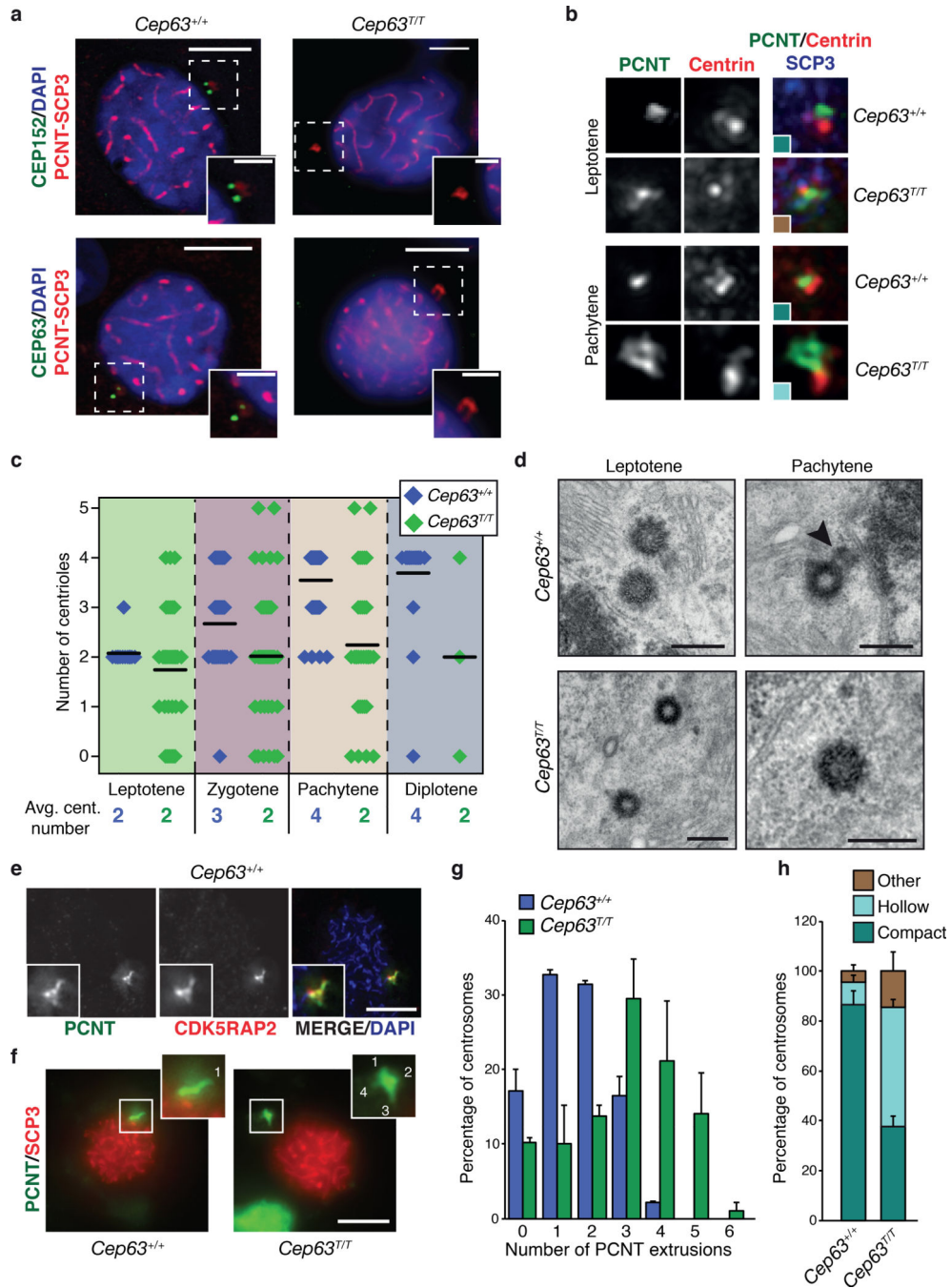**Figure 6. Centriole duplication failure during meiotic prophase I in *Cep63^{T/T}* mice**
(**a**) CEP152 and CEP63 are detectable at centrosomes, marked by PCNT, in the SCP3 staged prophase I cells of WT (left panels) but not *Cep63^{T/T}* (right panels) (scale bars represent 5 μm (left) and 2 μm (right)). (**b**) Example images of centriole configurations detected by immunofluorescence microscopy in spermatocytes at the indicated stage and of the indicated genotype. The colors of the insets correspond to the colors used for the graph in panel **h**. (**c**) Quantification of centriole numbers in prophase I spermatocytes at the indicated stage and of the indicated genotype. Example images are shown in panel b and in Supplementary Fig. 5.

Average centriole number per stage is indicated (black line) and the value rounded to a whole number shown numerically below (3 animals per genotype used, $Cep63^{+/+}$ n = 121, $Cep63^{T/T}$ n = 130 cells scored). (**d**) TEM analysis of centriole configurations in *WT* and $Cep63^{T/T}$ spermatocytes at the indicated stages. The arrowhead points to a daughter centriole growing from the wall of the mother (scale bar = 400 nm). (**e**) Co-distribution of the two PCM markers PCNT and CDK5RAP2 in squashes of *WT* spermatocytes. SCP3 staining was used for staging. (**f**) Examples of PCM extrusion patterns detected by PCNT staining in *WT* and $Cep63^{T/T}$ spermatocyte squashes. SCP3 staining was used for staging. The insets show magnifications of the PCM region, with extrusions labeled by numbers (scale bar = 5 μm). (**g**) Quantification of centrosome extrusions (PCNT staining) in spermatocytes of the indicated genotypes (n = 2 animals per genotype used, 92 $Cep63^{+/+}$ and 87 $Cep63^{T/T}$ cells scored). (**h**) Quantification of PCM distribution (PCNT staining) patterns in spermatocytes from *WT* and $Cep63^{T/T}$ mice (n = 3 animals per genotype used, 121 $Cep63^{+/+}$ and 130 $Cep63^{T/T}$ cells scored). Additional PCM marker analysis is included in Supplementary Fig. 6. All graphs with error bars are presented as the average plus standard deviation.
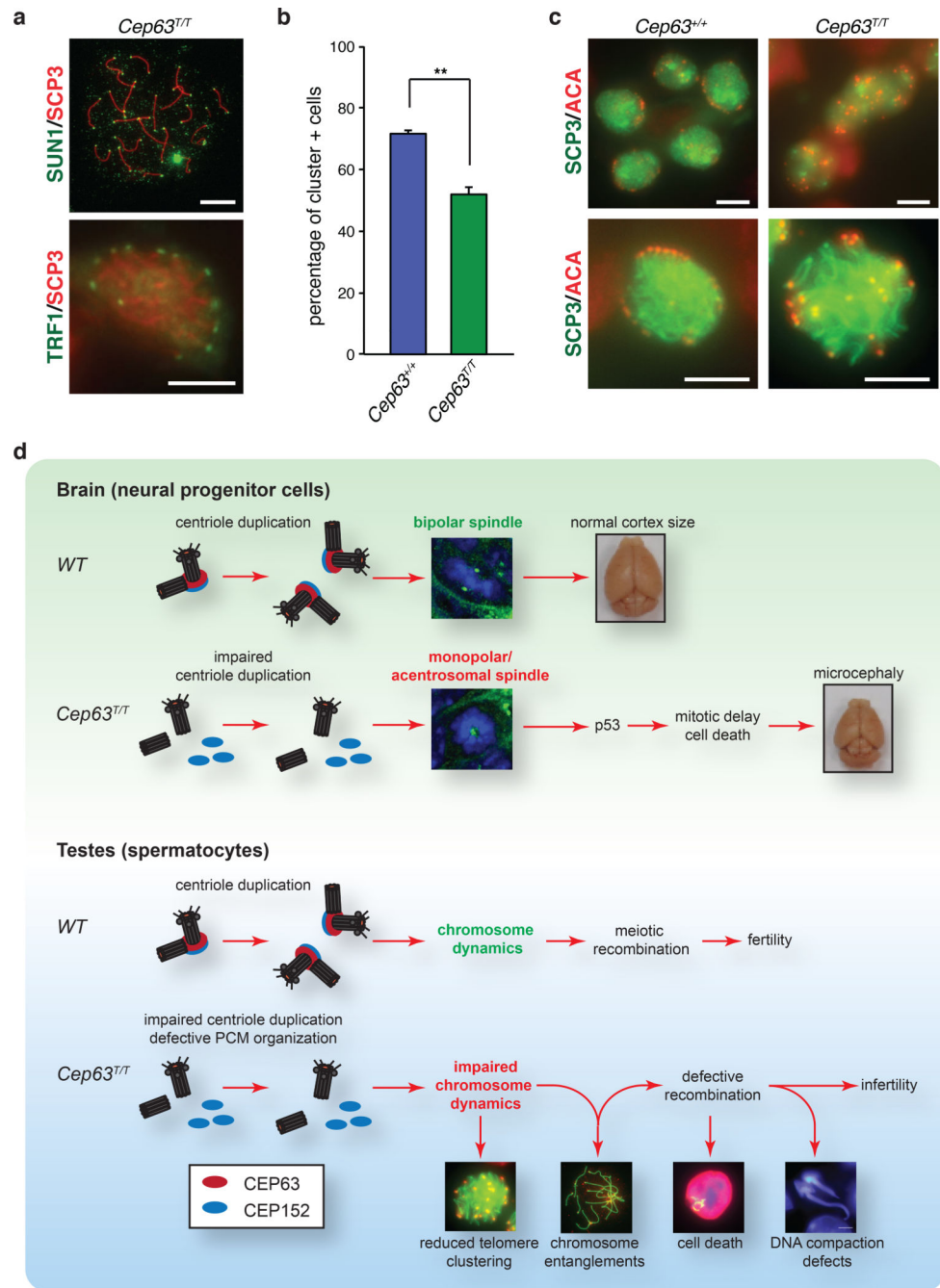
Figure 7. Reduced telomere clustering in *Cep63^T/T* mice

(**a**) Telomeric attachment in spermatocytes visualized by staining with SUN1 (top picture – pachytene spread, scale bar = 10 μm) or TRF1 (lower picture – equatorial plane from pachytene squash, scale bar = 5 μm). (**b**) Quantification of cells with clustered telomeres, indicative of bouquet formation, in p10 spermatocytes of the indicated genotype (*Cep63^+/+* n = 4 and *Cep63^T/T* n = 5 animals per genotype used, 274 and 407 cells scored, respectively). Graph with error bars shows the average plus standard deviation. Asterisks denote statistical significance (n.s.= not significant, * = p-value <0.05, ** = p-value < 0.01,

*** = p-value < 0.001) determined by an unpaired two-way Student's T-test. (**c**) Representative squash images from cells of the indicated genotype staining with ACA (centromere/telomere) and SCP3 (SC), scale bar = 5 μm. (**d**) Model of CEP63 function in normal brain and testes development. See text for description.